Supporting Information

A Two-Dimensional Bilayered Dion-Jacobson-Type Perovskite Hybrid with Narrow Bandgap for Broadband Photodetection

Dongying Fu,*[a] Jianrong Yuan,[a] Shichao Wu,[a] Yunpeng Yao,[b] Xinyuan Zhang,[b] Xian-Ming Zhang,*[a]

[a] *Institute of Crystalline Materials, Institute of Molecular Science, Shanxi University, Taiyuan, Shanxi 030006, China*

[b] *State Key Laboratory of Structural Chemistry, Fujian Institute of Research on the Structure of Matter, Chinese Academy of Sciences, Fuzhou, Fujian, 350002, P.R. China.*

**E-mail: dyfu@sxu.edu.cn (D. Fu), xmzhang@sxu.edu.cn (X.-M. Zhang)*

Table of Contents for Supporting Information

Experimental section

Synthesis and Crystal Growth. For the chemical synthesis of **1**, $Pb(CH_3COO)_2$ (0.758 g, 2 mmol) and methylamine (0.031 g, 1 mmol) were dissolved in 10 mL of HI (47%) solution by stirring for 10-15min. Then, 2-methyl-1,5-diaminopentane (0.116 g, 1 mmol) was added into mixed solution with continuous stirring and heating, until the solution turned clarifies. Red plate-like crystals precipitate during slow cooling to room temperature.

Powder X-Ray Diffraction Analysis. MiniFlex Ⅱ Powder X-Ray Diffractometer (PXRD) was used to check the phase purity of desired compounds. The experimental PXRD patterns were recorded in the 2theta (2θ) range of 5°-50° with a step size of 5°. The experimental PXRD patterns obtained at room temperature match fairly well with the calculated data based on the single-crystal structure, which solidly confirm the purity of the as-grown crystals of **1** (Fig. S1).

Structure Determination. Single crystal X-ray diffraction (SCXRD) was performed on D-8 diffractometer by using Mo-Kα radiation (λ= 0.71073 Å). Intensity data acquisition, data reduction and cell refinement were performed using the CrysAlisPro program. The structures of all desired compounds were solved by direct methods and refinements were made by the least-squares program. Table S1 summarizes the detailed information of crystal parameters, structure refinement and data collection.

Ultraviolet-visible (UV-vis) Absorption Spectrum. UV-vis diffuse reflectance spectroscopy of desired materials were performed at room temperature on Perkin-Elmer Lambda 900 UV-Vis spectrophotometer in a variable wavelength range between 200 to 1000nm. The $BaSO_4$ was used as the 100% reflectance reference, and the powdered crystals were used for the measurements.

Near the cut-off of the optical transmission, the band gap, the absorption and the wave frequency obey the equation: $\alpha hv = A(hv - Eg)^{n/2}$

where α, v, A, and Eg are absorption coefficient, light frequency, proportionality constant, and band gap, respectively. In the equation, n decides the characteristics of the transition in a semiconductor (n=1, indirect absorption; n=4, indirect absorption). The values of n and Eg were determined by the following steps: first, plot ln(αhv) vs ln(hv - Eg) using the approximate Eg value, and then determine the value of n with the slope of the straight line near the band edge; second, plot $(\alpha hv)^{1/n}$ vs hv and then obtain the band gap Eg by extrapolating the straight line to the hv axis intercept.

First-Principles Calculations. First-principles density function theory (DFT) calculations were performed with the Cambridge Sequential Total Energy Package (CASTEP).[1,2] Since the orientations of the $[2meptH_2]^{2+}$ cations in the structure exhibit random distribution, a proposed structure with all $[2meptH_2]^{2+}$ cations aligned along an ordered direction were used for calculation. The exchange-correlation energies were described by a generalized gradient approximation (GGA) with Perdew-Burke-Ernzerhof functional for solids (PBEsol) scheme.[3] The interactions between the ionic cores and the electrons were described by the norm-conserving pseudopotential.[4] The following orbital electrons were treated as valence electrons: Pb $6d^{10}$ $6s^2$ $6p^3$; I $5s^2$ $5p^5$; C $2s^2$ $2p^2$; N $2s^22p^3$ and H $1s^1$. The numbers of plane waves included in the basis sets were determined by a cutoff energy 320 eV. To achieve the accurate density of the electronic states, the *k*-space integrations were done with Monkhorst-Pack grids with a 6 × 6 × 3 *k*-point for compound **1**. The other parameters and convergent criteria were the default values of CASTEP code.

References

1. M. D. Segall *et al.* First-principles simulation: ideas, illustrations and the CASTEP code. ***J. Phys.: Condens. Matter*** 14, 2717-2744 (2002).
2. S. J. Clark *et al.* First principles methods using CASTEP. ***Zeitschrift Fur Kristallographie*** 220, 567-570 (2005).
3. J. P. Perdew *et al.* Restoring the Density-Gradient Expansion for Exchange in Solids and Surfaces. ***Phys. Rev. Lett.*** 100, 136406 (2008).
4. D. R. Hamann, Schlüter, M. & Chiang, C. Norm-Conserving Pseudopotentials. ***Phys. Rev. Lett.*** 43, 1494 (1979).

Photoelectric Responses and Conductivity. Photoelectric responses of **1** were tested on a current meter (Keithley6517B) by using lateral two-probe devices based on crystal samples under the wavelengths of 405 nm, 520, and 637 nm, respectively, and the photoelectric activity under simulated sunlight illumination was also measured. The I−V curves were also tested at a fixed voltage (10 V) at different temperatures; thus, their variable-temperature conductivities were calculated to range from 308 to 362 K.

Table S1. Crystal data and structure refinement for **1**

Empirical formula	$(C_6H_{12}N_2H_6)(CH_3NH_3)Pb_2I_7$
Temperature	250 K
Formula weight	1452.97
Crystallographic system	orthorhombic
Space group	*Cmcm*
Unit cell dimensions	a = 12.7220 (5) b = 12.5151 (5) c = 34.3778 (17) V = 5473.5 (4)
Z, Calculated density	8, 3.526 g/cm^3
F (000)	4976
Theta range for data collection	4.566 to 52.75 º
Limiting indices	$-14 \leq h \leq 15$ $-15 \leq k \leq 15$ $-40 \leq l \leq 42$
Reflections collected/unique	18789/2963 [R_{int} = 0.0820]
Completeness	99.4%
Data/restraints/parameters	2963/38/118
Goodness-of-fit	1.028
Final R indices [I>2sigma(I)]	R_1 = 0.0537, wR_2 = 0.1404

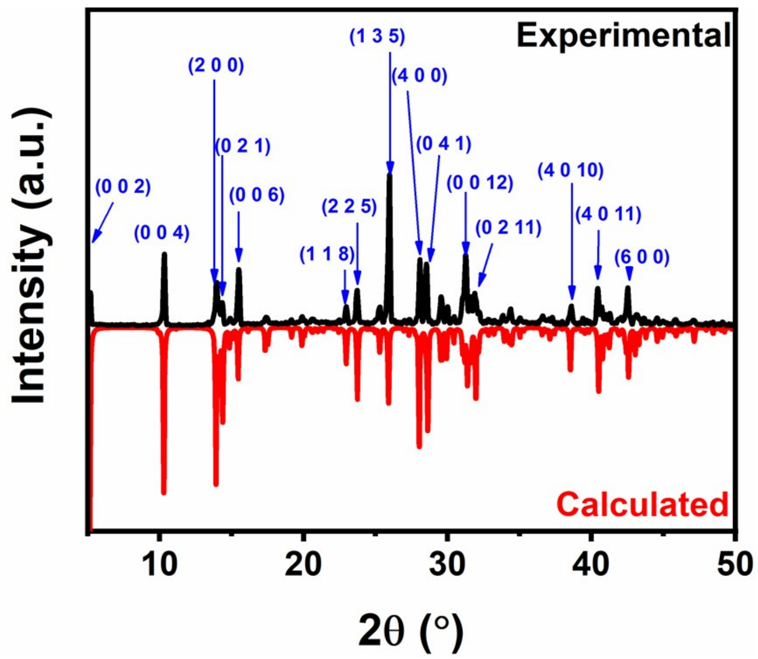

Fig.S1. Experimental and calculated PXRD patterns of **1** at room temperature.

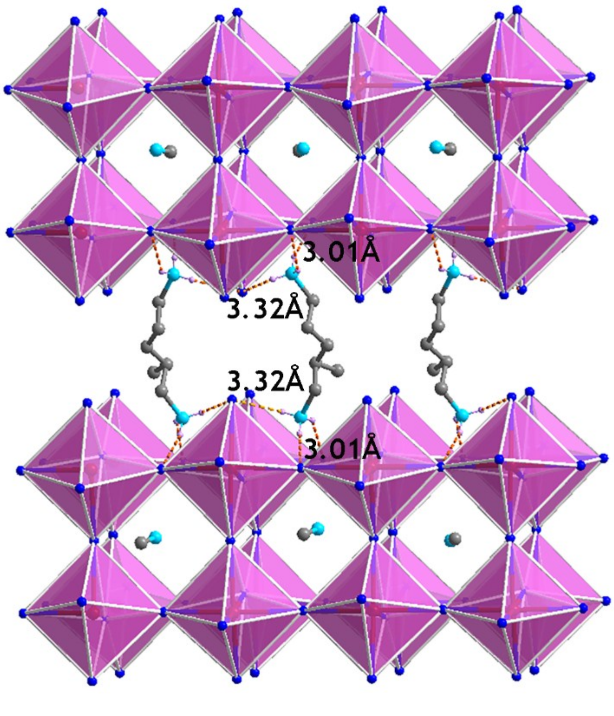

Fig. S2. H-bonds of $-NH_3^+$ groups of the divalent organic cations with the bridging I^- in compound **1**.

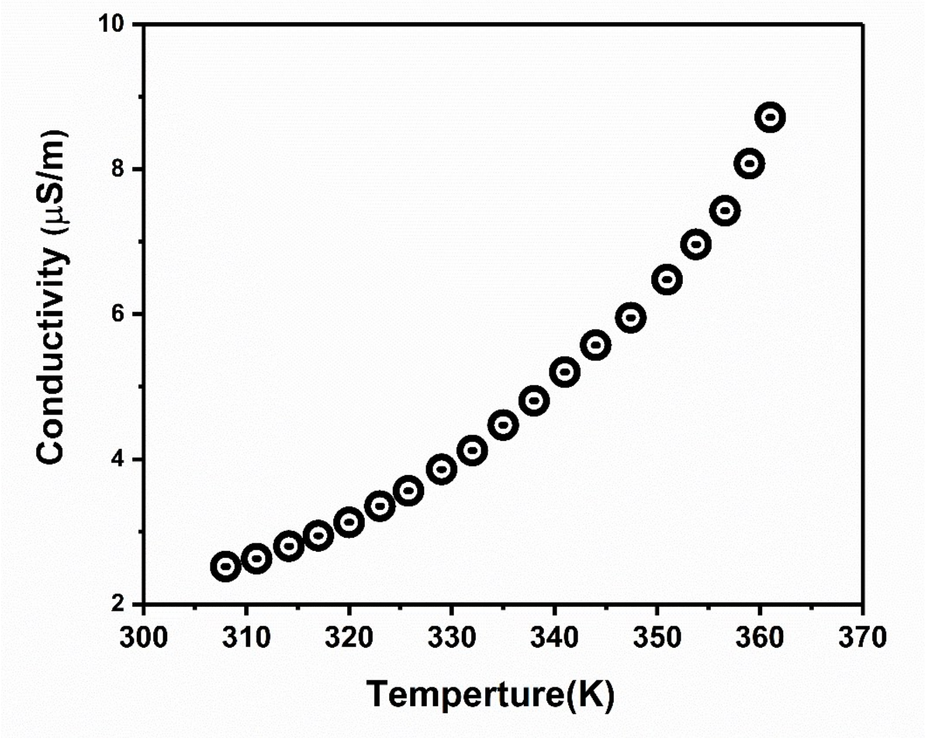

Fig. S3. Variable-temperature conductivity of **1**.

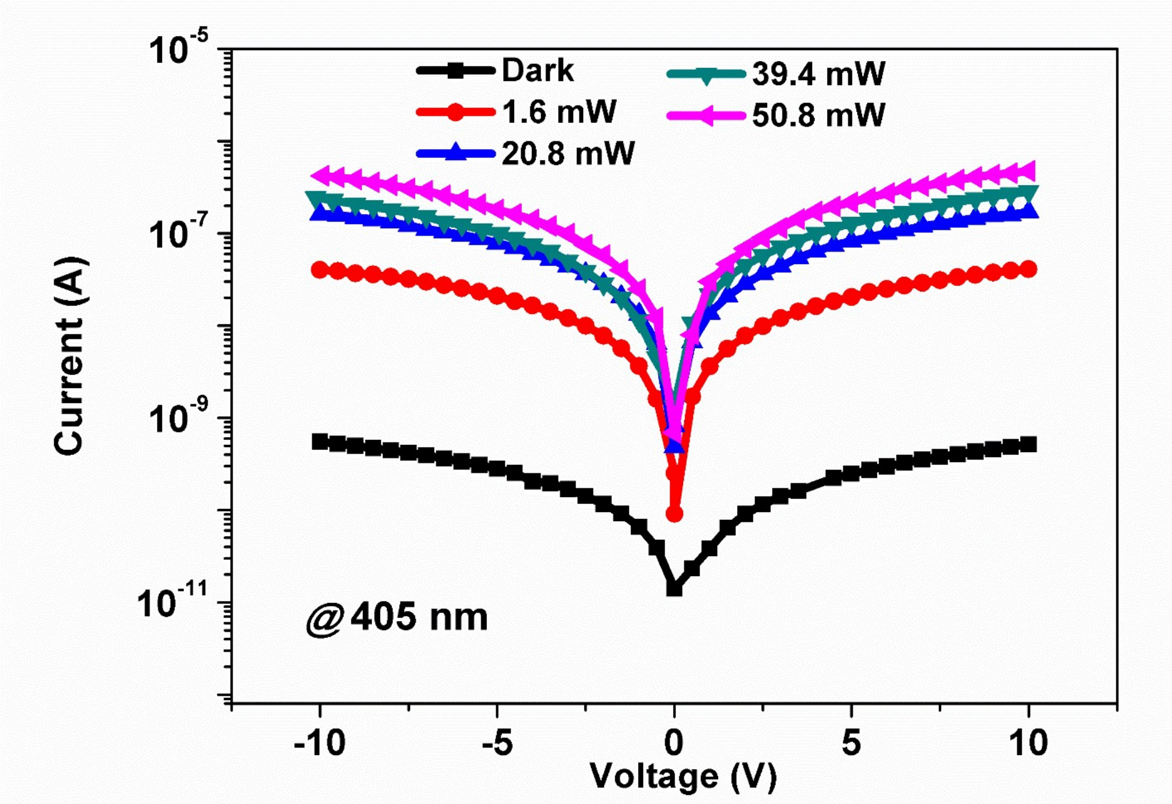

Fig. S4. The logarithmic *I*–*V* curves of the film detector measured in the dark and under different illumination intensities at 405 nm for **1**.

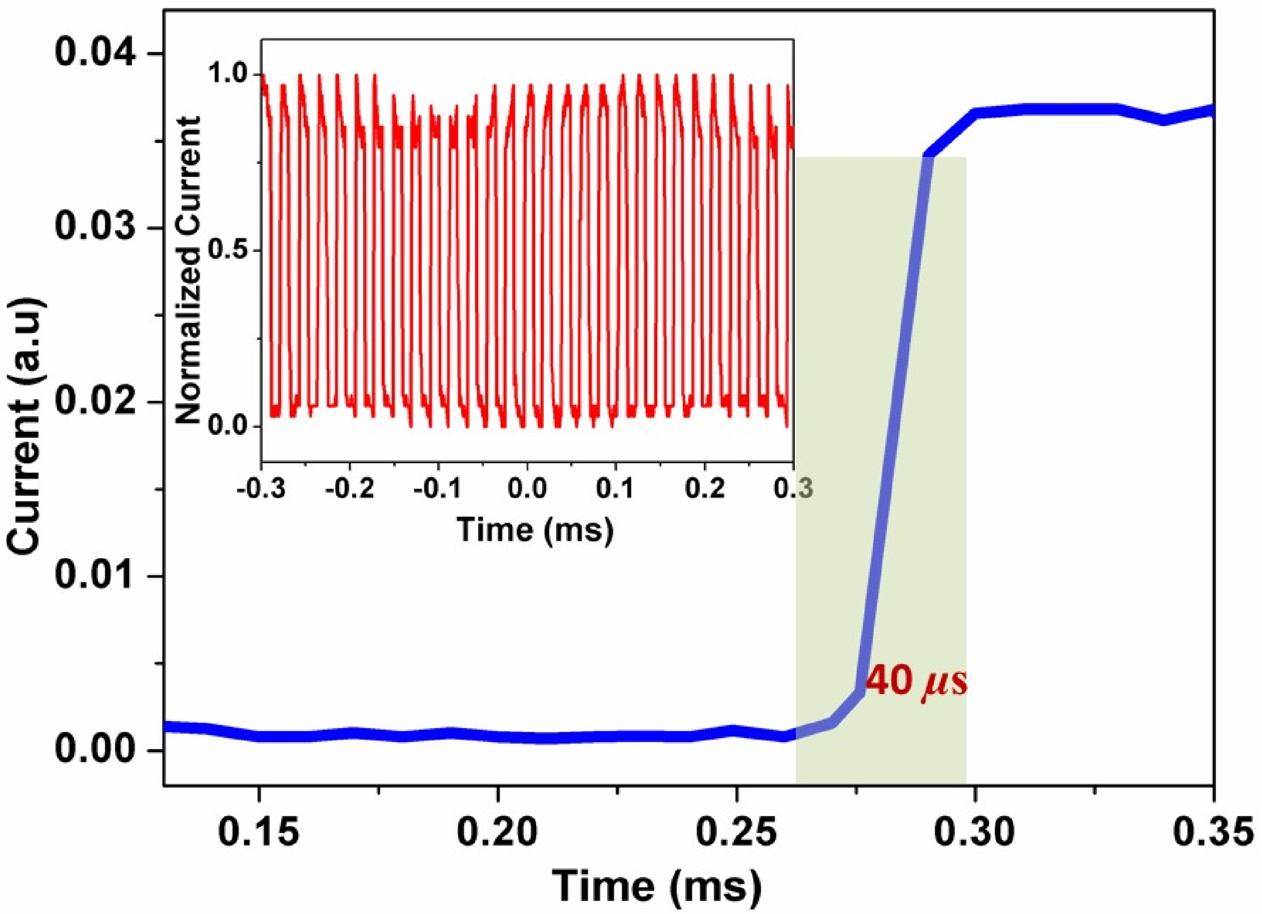

Fig. S5. Photocurrent response time of **1** (Insert: The long-time cyclability of photodetector for **1**.).

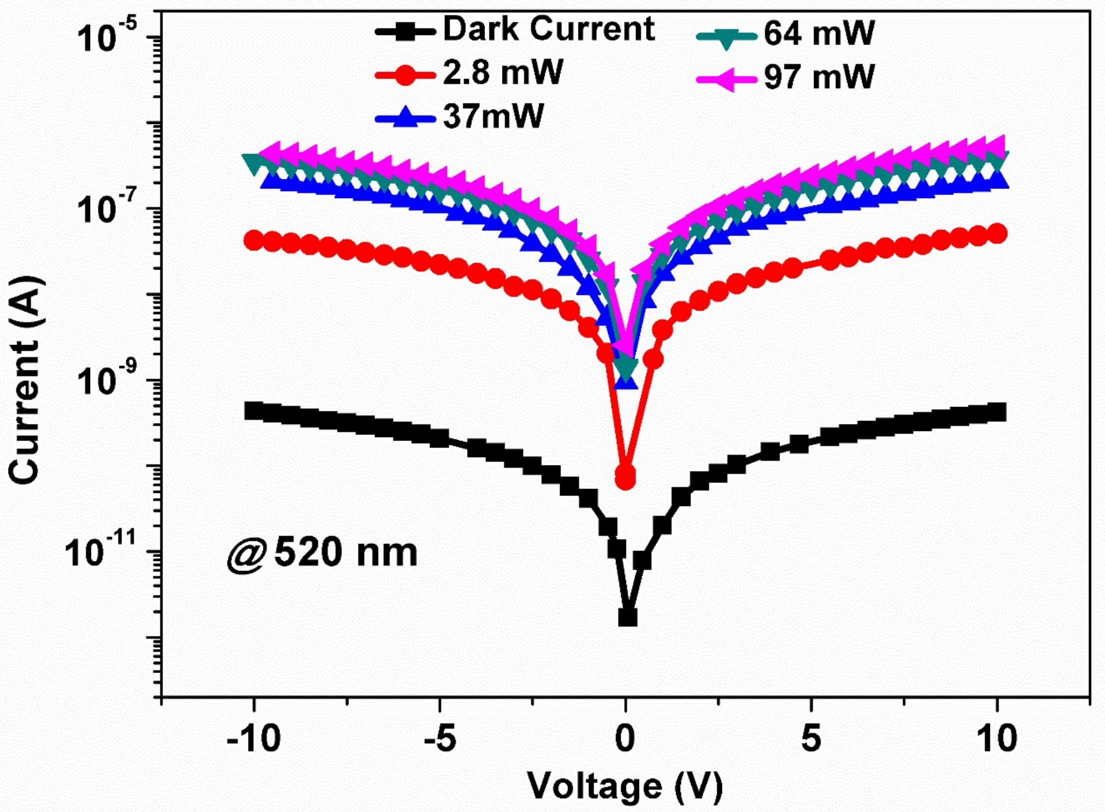

Fig. S6. The logarithmic *I*–*V* curves of the film detector measured in the dark and under different illumination intensities at 520 nm for **1**.

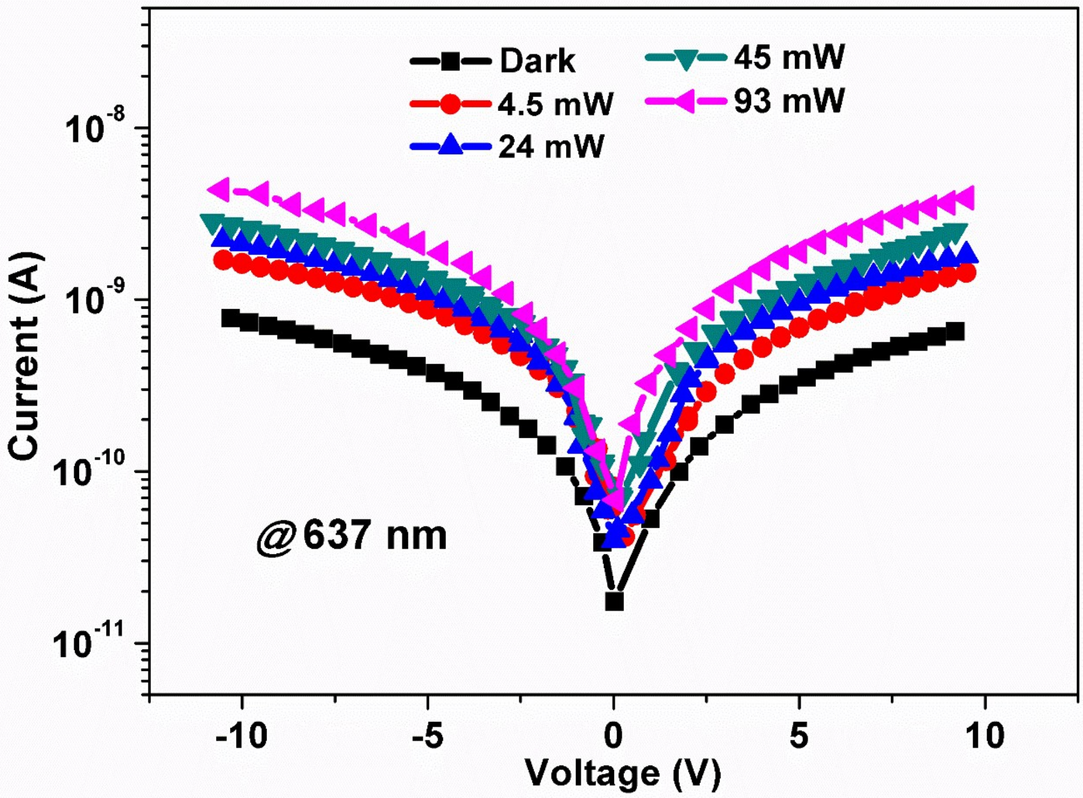

Fig. S7. The logarithmic *I*–*V* curves of the film detector measured in the dark and under different illumination intensities at 637 nm for **1**.

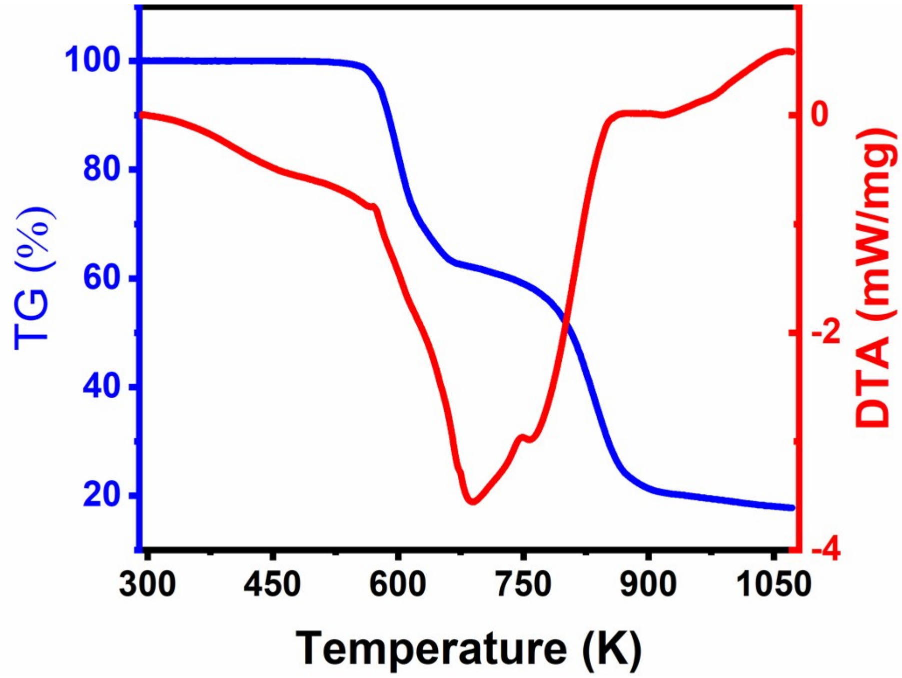

Fig. S8. The TGA/DTA results of **1**.

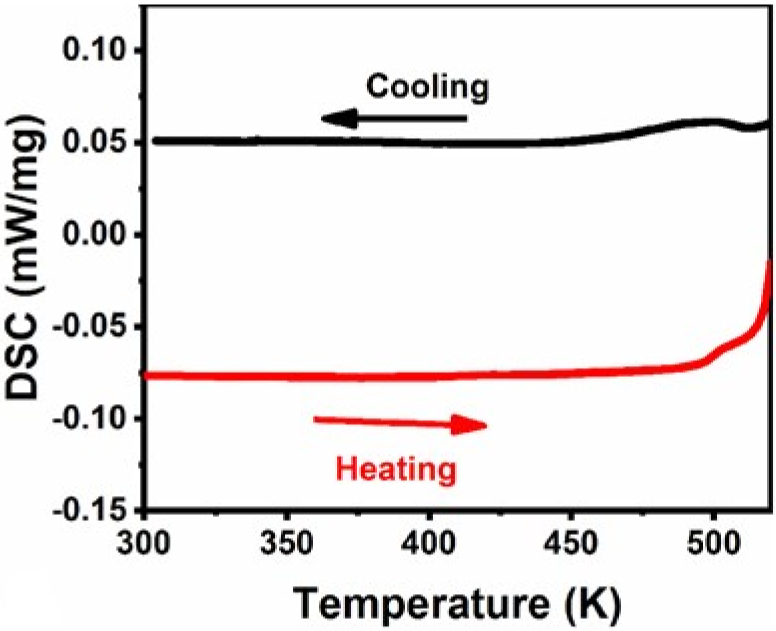

Fig. S9. DSC results of **1**.